Advanced defect classification by smart sampling, based on sub-wavelength anisotropic scatterometry

Van Der Walle, Peter; Kramer, Esther; Ebeling, Rob; Spruit, Helma; Alkemade, Paul; Pereira, Silvania; Van Der Donck, Jacques; Maas, Diederik

Important note
To cite this publication, please use the final published version (if applicable).
Please check the document version above.

PROCEEDINGS OF SPIE

Advanced defect classification by smart sampling, based on sub-wavelength anisotropic scatterometry

Peter van der Walle, Esther Kramer, Rob Ebeling, Helma Spruit, Paul Alkemade, et al.

SPIE.

Advanced defect classification by smart sampling, based on sub-wavelength anisotropic scatterometry

Peter van der Walle[* 1], Esther Kramer[1], Rob Ebeling[1], Helma Spruit[1],
Paul Alkemade[2], Silvania F. Pereira[2,] Jacques van der Donck[1], Diederik Maas[1]

[1]TNO, 2626CK Delft, Netherlands
[2]Delft University of Technology, Faculty of Applied Sciences
Lorentzweg 1, 2628 Delft, The Netherlands

ABSTRACT

We report on advanced defect classification using TNO's RapidNano particle scanner. RapidNano was originally designed for defect detection on blank substrates. In detection-mode, the RapidNano signal from nine azimuth angles is added for sensitivity. In review-mode signals from individual angles are analyzed to derive additional defect properties. We define the Fourier coefficient parameter space that is useful to study the statistical variation in defect types on a sample. By selecting defects from each defect type for further review by SEM, information on all defects can be obtained efficiently.

Keywords: Particle contamination, defect detection, defect review, advanced defect classification, redetection, semiconductor, latex sphere equivalent, dark field microscopy, scatterometry, ADC, SEM

1. INTRODUCTION

Particle defects are a significant contributor to yield loss in semiconductor manufacturing. To determine the origin of and, in the end to control particle defects, the presence, shape, size and composition of these particles must be characterized. Advanced Defect Classification (ADC) is an established technique to pursue defectivity control[1]. With shrinking device dimensions, increasingly smaller particles become the root cause for device failure by critical defects. This strongly raises the challenge for defect detection and review tools, as both more and smaller particles need to be found and analyzed. This paper extends our previous feasibility study[2] of using optical metrology by sub-wavelength anisotropic scatterometry as a first step in ADC. By performing optical defect review during or right after optical inspection, information on present defects is available earlier in the review process. We have developed an algorithm to quantitatively classify defects based on this information. This initial classification can subsequently be used to select a sample of defects for review on slower high-resolution review tools, such as SEM, HIM and AFM, making the defect review process more efficient.

Since defects occur at low densities, the first step in defect classification is detection and assignment of accurate coordinates to the defect. Optical metrology is the only technique with a high enough throughput for this step. TNO has developed the RapidNano 3 particle scanner for this purpose[3]. This scanner (RN3) is capable of detecting 42 nm PSL particles on highly polished substrates. This high sensitivity is achieved by reducing the background variance by illuminating the sample from multiple azimuth angles[4]. In detection mode (RN3.1), the signals from all azimuth angles are added and a defect is detected when this sum exceeds a certain threshold value. The multi-azimuth illumination can also be used for defect review. In this mode (RN3.9), the signal from the 9 azimuth angles is recorded individually. The differences in scattering intensity as a function of azimuth angle are analyzed to extract additional information on the defect. In detection mode, the defect location and estimated size are determined, while in review mode also aspect-ratio, skewness and orientation are reconstructed.
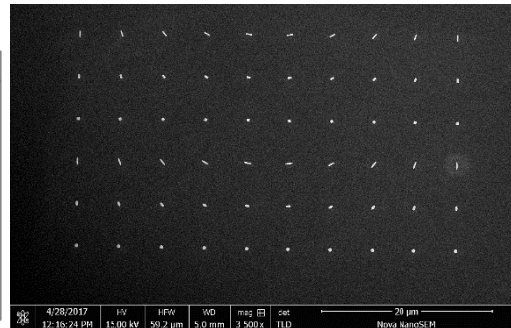
2. EXPERIMENTAL

The Rapid Nano particle scanner has 9 illumination angles. The illumination is switched between the 9 illumination arms by a wheel with 16 mirrors and a final fixed mirror. Each arm has two mirrors on the wheel to keep the wheel balanced. In detection mode this wheel spins at 1200 RPM and the camera exposure time is set to a multiple of 25 ms, i.e., half the revolution period of the wheel. In this way, the camera records an image that corresponds to the sum of the images, each with illumination from one arm. After each (sum) image, the substrate is moved to the next position until the recorded images cover the entire detection surface.

In review mode, a detected defect is moved to the center of the image. The wheel is set stationary and for each mirror position an image is recorded. The exposure time is set such that on average the scattered energy will reach 25% of the dynamic range of the camera. A small area around the center of the image is integrated to determine the scattering cross-section for each illumination arm expressed in gray-value per Joule illumination energy (gv/J).

Samples with programmed defects were fabricated by e-beam lithography. Arrays of elliptical and rectangular defects were written in CZAR[5] resists at 5 different sizes, 3 different aspect-ratios and 9 different orientations. After development, the defect shapes were either etched 20 nm into the wafer or deposited on top of the wafer via a lift-off process. The dimensions of the fabricated defects were verified by both SEM (FEI Nova NanoSEM 650) and AFM (Bruker Dimension FastScan) inspection. A set of markers for easy navigation and redetection was added to the wafer in the same process steps[6].

Table 1 Left: Overview of the variable programmed defect design parameters. Right: SEM image of a set of defects

2D shape	Aspect ratio (1 : AR)	Size parameter: D (nm)	Rotation (°)
Ellipse	1:1	60	0 / 180
Rectangle	1:2	80	20 / 200
	1:5	100	40 /220
		200	60 / 240
		400	80 / 260
			100 / 280
			120 / 300
			140 / 320
			160 / 340

The detection step for these programmed defects was skipped as the location of the defects was already known from the sample design. The design coordinates of all defects were transformed to the stage coordinates of the Rapid Nano by finding the stage coordinates of 3 markers on the wafer. Optical defect review was performed for all 3000 defect locations.

Figure 1 shows the polar plots of the 9 azimuth scattering cross-sections for 3 rectangular defects at different aspect-ratios in the top row. The middle row shows the SEM images of the same defects, while the bottom row shows 2 AFM measurements on the same defects.
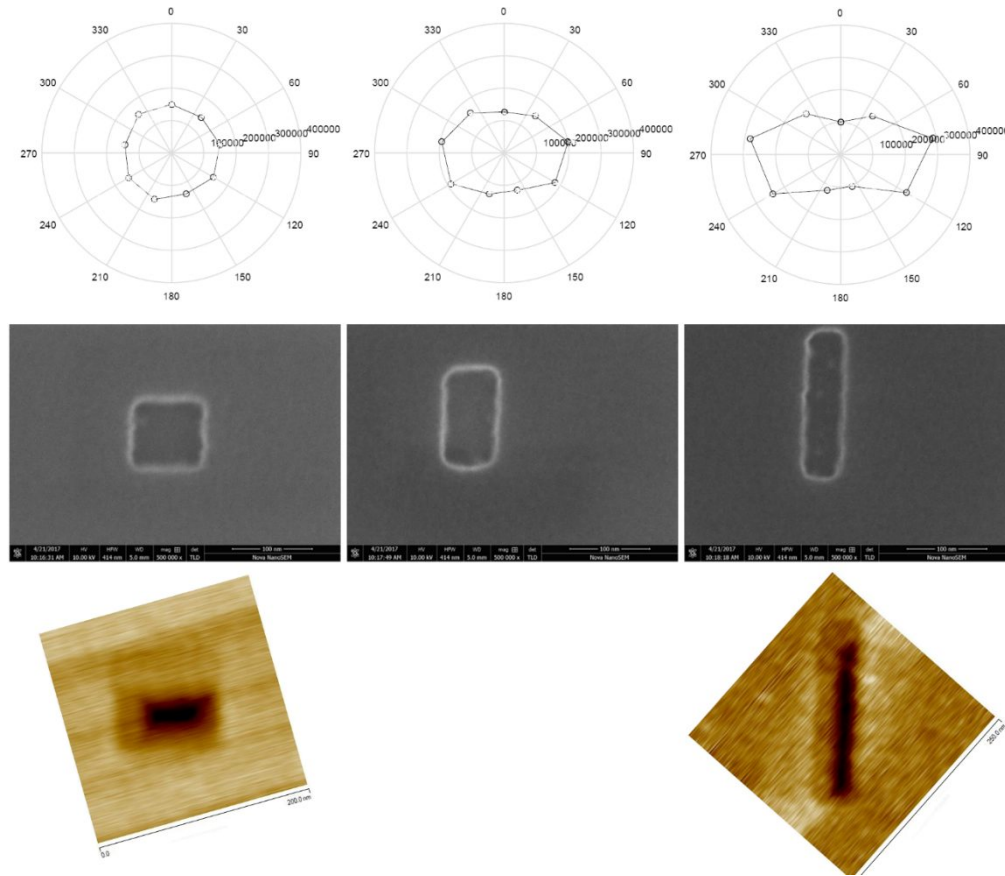
Figure 1: Optical signal strength (gv/J) as measured using RN3.9 for 9 angles distributed around 360 degrees scattering directions (top row) and SEM (center row) and AFM (bottom row) images, all from the same re-detected programmed defects. The design size of the square defects is CD = 100 nm, with aspect ratio AR = 1:1 (left column), 1:2 (center column) and 1:5 (right column). The defect volume is kept constant.

3. SMART SAMPLING

In review mode, the Rapid Nano yields 9 measurement values on a defect instead of 1. While this additional data is far from sufficient to determine the exact defect shape and material, it is a significant increase of information prior to high-resolution review. The statistical variance of defect types present on a sample can be better assessed with this data. We present a parameter space, the Fourier coefficient representation, that is particularly useful to study this variance. When clusters of data-points are present in these coefficients, a much improved selection of defects can be made for further high-resolution review. This selection can be made to equally cover all defect types present on the sample.

Fourier coefficient representation

Optical defect review yields 9 scattering cross-sections, one for each illumination azimuth of the Rapid Nano particle scanner. By plotting these values in a polar plot qualitative properties of the defect can be visualized (Figure 1). e.g., elongated defects show an elongated polar plot, however with the long axis rotated by 90 degrees. The scattering of an elongated defect is strongest when the illumination is perpendicular to the long axis of the defect.

We transform the 9 measurement values for a single defect to more practical values by taking the Fourier transform over the azimuth angle. This transform yields one real and 4 complex numbers (k = [0..4]):

$$A_k = \sum_{n=0}^{8} S_n \cdot e^{-i2\pi kn/9},$$ (1)

where S_n are the 9 scattering cross-sections measured with the illumination azimuth at 40 degrees intervals. The 0th order coefficient A_0 is equal to the average of the 9 scattering cross-sections. The magnitude of the 1st order coefficient A_1 describes the skewness of the polar plot, while the phase corresponds to the direction of the skewness. Similarly, the magnitude of A_2 represents the aspect-ratio of the defect and its phase the orientation of the short axis.

The Fourier coefficient parameter space is a more useful space to represent the optical metrology data than the original 9 scattering cross-sections. Similar defects have similar magnitudes of the Fourier coefficients, but can have very different values for the direct measurement when the orientation of the defect is different. By having a representation in which similar defects are close, clusters in the defect data can be found. When the presence of such clusters is known, the high-resolution review can be done more efficiently, e.g., a few defects of each cluster can be selected for review to obtain information on all defects in these clusters.

As an example of this approach, we have performed optical review on a sample with programmed defects. This sample contains ellipses and rectangles of different sizes and aspect-ratios, see Table 1. From this design, it is clear that the 0th and 2nd order Fourier coefficients will be the most relevant. In a scatter plot with the magnitudes of these two parameters, 15 clusters show up, corresponding to the 3 different aspect-ratios and 5 different sizes of the investigated programmed defects. The rectangular (red) and elliptically shaped (blue) defects can't be separated by these two parameters. The center of all clusters was determined by a k-means algorithm and a Voronoi diagram was generated from these points as shown in Figure 2.
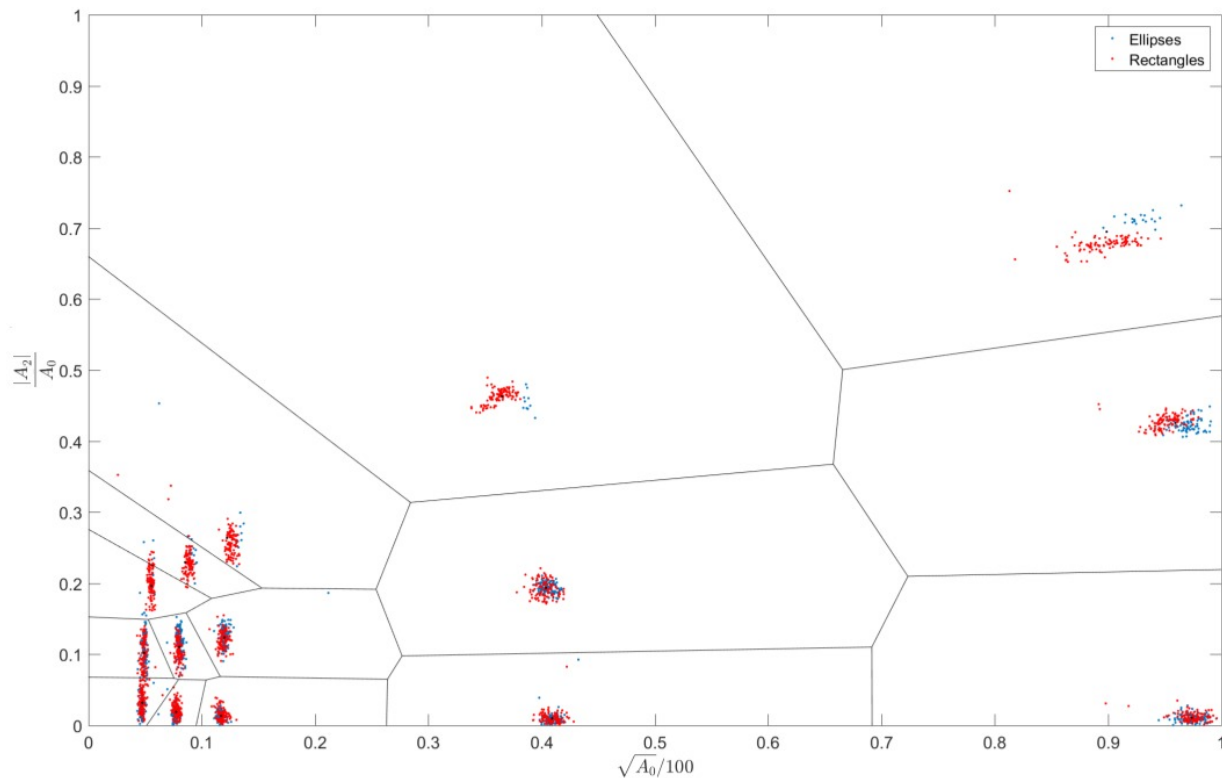

Figure 2 Scatter plot of the 2nd order versus 0th order Fourier coefficient of the scatterometry data for the 3000 programmed defects as defined in Table 1. Each cluster of data points can be related to a class within the set of programmed defects, e.g. the 3 clusters at the far left correspond to the 60-nm defects with aspect ratios of 1, 2, and 5 from bottom to top.

An alternative way to use the Fourier coefficients is to look at the phase. Figure 3 shows a polar plot of the 0th order coefficient versus the phase of the 2nd order coefficient. The 5 different sizes are well distinguishable, as the 5 rings in the polar plot. For the defects that have a well-defined orientation, i.e., with aspect-ratio 1:2 or 1:5, the 9 orientations present on the sample show as clusters of data points. This orientation sensitivity may be useful to classify defects that occur in well-oriented pattern such as bridges or gaps in dense lines.

We have shown two different ways to view the Fourier coefficients of the 9 azimuth scattering cross-sections of the programmed defects. These views focus on different aspects of the present defects. Each production process will have different associated defect types. By investigating various views of the optical metrology data, the presence of these different defect types can be detected. This information can be used to make the defect review process more efficient.
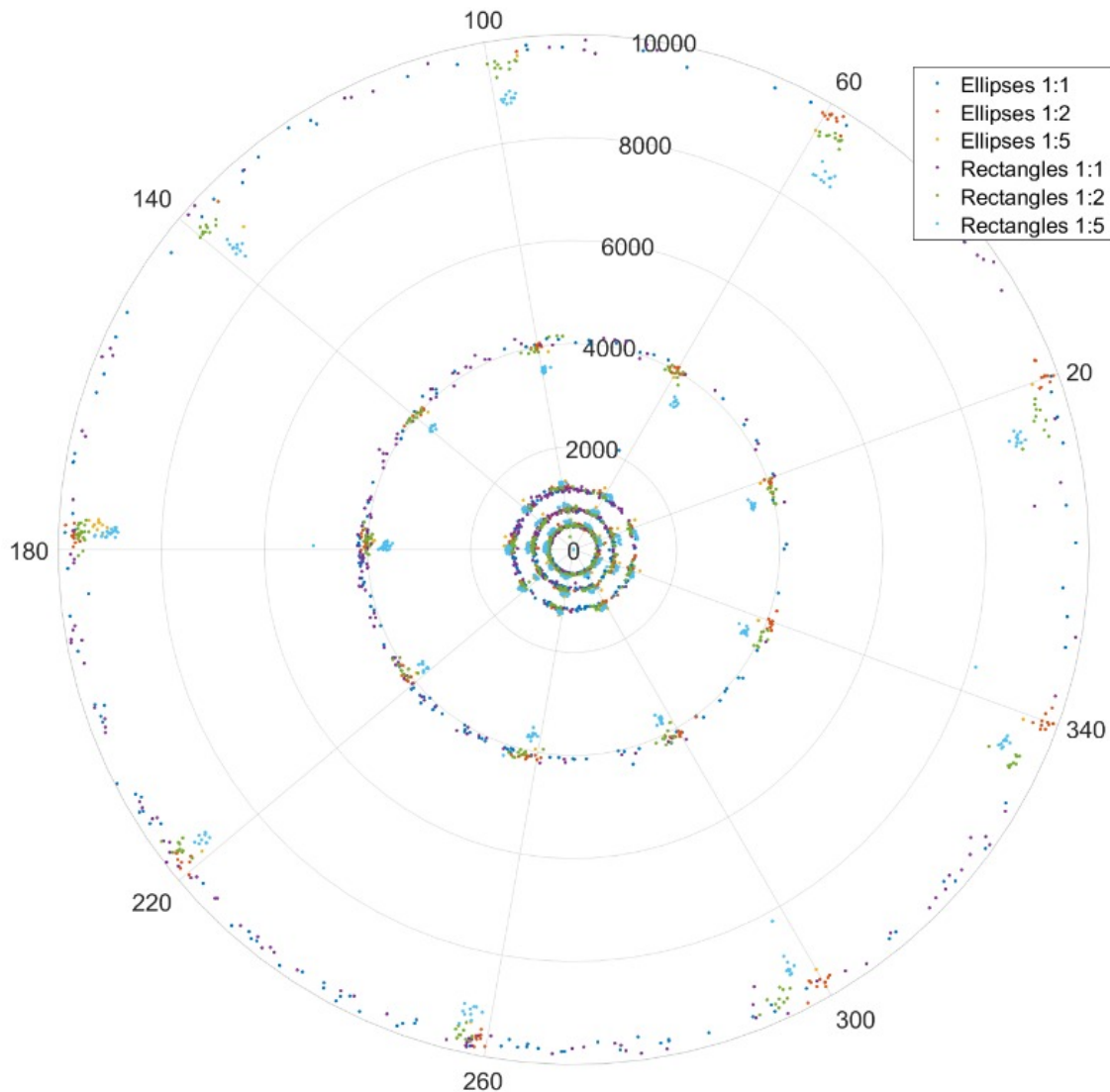

Figure 3 Polar plot of the RN3.9 signal (gv/J) versus the phase of the 2nd order coefficient A_2 of the Fourier transformed scatterometry data for the 3000 programmed defects as defined in Table 1. Defects of similar size but with a different shape show up at approximately the same radius. Defects with a clear orientation show up at the corresponding angle.

4. CONCLUSIONS

The Rapid Nano particle scanners' unique multi-azimuth illumination can be used to collect additional data on defects, beyond a size and location estimate. This data can be analyzed to determine the variance in defect type on a sample and find groups of defects that are likely of a single type. With this initial grouping in potential defect types, a smarter defect sampling can be achieved, such that more information on all defects on the sample is obtained in less time. Hence, this method makes more effective use of expensive defect review equipment such as SEM, HIM or AFM.

We have presented the Fourier coefficient representation of the multi-azimuth scattering cross-section data. It is particularly useful for analyzing the variance of defect types. The usefulness of this representation has been demonstrated on a programmed defect sample containing several defect types of different sizes, aspect-ratios and orientations. The complex character of the Fourier coefficients can be used for instance to focus on orientational effects or to completely discard them.

REFERENCES

[1] Boettiger, T., Buck, P., Paninjath, S., Pereira, M., Ronald, R., Rost, D., Samir, B., "Automatic Classification of Blank Substrate Defects", Proc. SPIE 9235 (2014) 92351J.
[2] van der Walle, P. et al., Deep sub-wavelength metrology for advanced defect classification, SPIE Optical Metrology, 103294N-10 (2017).
[3] van der Donck, J. et al., RapidNano: Towards 20nm Particle Detection on EUV Mask Blanks, MRS Advances, 1 (2016) 2225–2236. doi: 10.1557/adv.2016.299.
[4] van der Walle, P. et al., Implementation of background scattering variance reduction on the Rapid Nano particle scanner, SPIE Proc. 9048 (2014).
[5] Allresist. Positive e-beam resists ar-p 6200 (csar 62). Datasheet (2017).
[6] Bouwens, M.A.J. et al., Enhancing re-detection efficacy of defects on blank wafers using stealth fiducial markers, Microelectronic Engineering, 153 (2016) 48-54.